$^3H(\alpha,^6Li)n$ reaction at 0° *

Ronald E. Brown,† G. G. Ohlsen, R. F. Haglund, Jr., and Nelson Jarmie
Los Alamos Scientific Laboratory, University of California, Los Alamos, New Mexico 87545
(Received 22 February 1977)

We have measured excitation functions for the reaction $^3H(\alpha,^6Li)n$ at 0° (lab) in an energy range covering the resonance corresponding to the $5/2^-$ state in ^7Li at 7.46 MeV of excitation. A Ti-tritide target on a nickel backing was bombarded by an α-particle beam, and the ^6Li reaction products at 0° were spatially separated from the beam in a magnetic field and were then detected in a thin solid-state detector. Data at 14 bombarding energies were obtained for the ^6Li group emitted at $\theta_{c.m.} = 0°$, and data at 11 energies were obtained for the ^6Li group emitted at $\theta_{c.m.} = 180°$. To normalize these reaction data we measured, simultaneously with the reaction, the yield of the elastically recoiling tritons at $\pm 15°$ and $\pm 30°$ (lab). We obtained absolute differential cross sections from the normalized reaction data by measuring excitation functions for $^3H(\alpha,t)^4He$ at 15° and 30° (lab) using a gas target. The average error in the reaction data is 2.7%; the errors in the 15° elastic data are less than 1%; the majority of the errors in the 30° elastic data are less than 2%; and the α-particle beam energy at the reaction region of the targets was determined to an accuracy of 6 keV. Our reaction data are compared with other data, data evaluations, and a recent three-channel multilevel R-matrix analysis of a large body of mass-7 data.

[NUCLEAR REACTIONS $^3H(\alpha,^6Li)n$, $^3H(\alpha,t)^4He$, $E=11.3$–12.0 MeV; measured reaction $\sigma(E;0°)$, elastic $\sigma(E;15°, 30°)$. Comparisons with other data, with data evaluations, and with three-channel, multilevel, R-matrix analysis.]

I. INTRODUCTION

Much effort has been devoted over the years to the study of the interaction of ^6Li with neutrons, and discussions of recent work and reviews of older work are given in Refs. 1–3. Practical aspects of the $n+^6Li$ interaction have stimulated many of these studies. For example, the $^6Li(n,t)^4He$ reaction is often used as a neutron-detection standard for neutrons of energy below about 100 keV (Refs. 4–6) and has been used at higher energies to monitor reactor neutron spectra.[7] The same reaction might also be used for breeding tritium in fusion reactors by incorporating a lithium blanket in the first wall.[8,9] Knowledge about the $n+^6Li$ interaction is also important for a basic understanding of the mass-7 system through theoretical studies, such as resonating-group calculations,[10] which employ a nucleon-nucleon force and fully antisymmetrized wave functions, or through more phenomenological approaches, such as R-matrix analyses.[11–14]

In the neutron energy range from about 100 to 500 keV, the $n+^6Li$ interaction is dominated by a resonance which causes cross sections to peak near a neutron energy of 240 keV. This resonance is the one labeled $^4P_{5/2}$ in the study of $\alpha+t$ elastic scattering by Spiger and Tombrello[15] and arises from the influence of the $\frac{5}{2}^-$ state at an excitation of 7.46 MeV in ^7Li. In this energy region the experimental data exhibit large discrepancies. For example, the discrepancies in the angle-integrated cross section for $^6Li(n,t)^4He$ are strikingly illustrated in Fig. 2 of the review article of Uttley *et al.*[4] Because $\alpha+t$ is the only open reaction channel in this resonance region, the observation[4,12] that adopted values for the $n+^6Li$ total, angle-integrated elastic, and $\alpha+t$ reaction cross sections often are inconsistent with one another is cause for concern. Such an inherent "violation of unitarity" in the experimental data will naturally cause difficulties for analyses of such data with unitary theories, as, for example, the R-matrix analyses of Refs. 12–14.

It seems clear, then, that data are still needed on the $n+^6Li$ interaction and that it would be valuable to attack the problem in a novel way rather than to make yet another set of measurements employing methods and techniques used previously. We have satisfied the objective of novelty in the present experiment by obtaining differential cross sections for the $^6Li(n,t)^4He$ reaction at c.m. angles of 0° and 180° by measuring the reaction $^3H(\alpha,^6Li)n$ at 0° (lab). In this way we have replaced the set of problems associated with neutron beams or neutron detection by the set associated with charged-particle beams and charged-particle detection. These $^3H(\alpha,^6Li)n$ excitation functions were measured in the energy region of the above-mentioned $\frac{5}{2}^-$ resonance. Our results are compared with other data, with data evaluations, and with a recent three-channel, multilevel, R-matrix

analysis[16] of a large body of mass-7 data in which the present results were not included.

II. EXPERIMENT

A. Overview

Our method of measurement of the $^3H(\alpha,{}^6Li)n$ reaction cross section required that we also measure the $\alpha + t$ elastic scattering cross section. Both experiments were performed at the Los Alamos Van de Graaff facility, using an α-particle beam from the FN tandem accelerator. The reaction experiment used a Ti-tritide target on a Ni backing, and the elastic-scattering experiment used a tritium gas target.

The energy of the $\frac{5}{2}^-$ resonance in ^7Li, near which we made our measurements, is not far above the lab threshold energy E_{th} for ^6Li production (E_{th} = 11.136 MeV); therefore, the ^6Li ions from the reaction are produced in the laboratory in a narrow forward cone. At the cross-section peak, which occurs at about E_α = 11.61 MeV, the cone half angle is about 4°. This makes it difficult to measure the angular distribution of the ^6Li ions, and it was decided to measure only differential cross sections at 0° (lab). The ^6Li detection system could then readily be aligned along the direction defined by the beam-line collimating apertures. This detection system consisted of a simple dipole magnet, used to separate ^6Li ions from beam α particles, and a solid-state detector of thickness about equal to the range of the detected ^6Li ions. We detected two energy groups of ^6Li in this experiment. One group, having an energy of about 6.5 MeV, arises from emission at a c.m. angle of 0°, and the other group, having an energy of about 4.9 MeV, arises from emission at a c.m. angle of 180°. Measurements necessary to obtain information on ^6Li charge-state probabilities were also made in the course of data taking. In order to normalize the 0° reaction data, the yield of tritons from $^3H(\alpha,t)^4He$ scattering was monitored at ±15° and ±30° (lab) simultaneously with the 0° measurements.

The normalized reaction yields for $^3H(\alpha,{}^6Li)n$ can be converted to absolute differential cross sections if one knows the absolute differential cross sections for $^3H(\alpha,t)^4He$ elastic scattering. The needed elastic scattering cross sections were measured in a separate gas-target experiment. Because, in the resonance region of our measurements, the cross sections vary rapidly with energy, it was necessary to match carefully the energies in the two separate experiments. The use of two monitor angles, rather than only one, facilitated the energy matching, because the ratio of the 15° to 30° elastic cross section is a sensitive function of the α-particle bombarding energy. Hence, the energy matching was carried out by comparing the 15°/30° elastic-yield ratios obtained during the reaction measurements with those obtained during the elastic-scattering measurements. This then allowed us to use the 15°, elastic, absolute differential cross section to obtain absolute cross sections for the reaction. The 15°, rather than 30°, data were used for the conversion to absolute cross section because of their higher overall accuracy.

In addition to this energy-matching procedure, an absolute energy scale for the reaction measurements was determined by a special calibration of the tandem beam-analyzing magnet and by a measurement of the beam energy loss in the solid target. All the data were corrected for finite geometry, multiple scattering, and beam energy spread.

B. Elastic scattering: Apparatus and procedure

For the $^3H(\alpha,t)^4He$ elastic scattering experiment, a 76.2-cm-diam scattering chamber and its associated gas-target apparatus were used. This system and data-taking procedure are described in detail in Refs. 17 and 18, and some comments pertinent to the use of tritium as a target gas are made in Ref. 19. In brief, the α-particle beam passed through a tritium gas target having 2-mg/cm^2 Havar[20] foil windows and was collected in a Faraday cup having both magnetic and electrostatic electron suppression. A single, collimated, ΔE-E mass-identifier detector system was used to measure the yield of elastically recoiling tritons from the target. Each of the two geometry-defining collimators were nominally 3.5 mm wide and were separated by 222 mm. The rectangular rear collimator was about 5.9 mm high and was 305 mm from the chamber center. This results in a nominal geometry factor[21,22] of 1.07×10^{-3} mm sr and in an angular acceptance of about 0.9° [full width at half maximum (FWHM)] in the scattering plane. Measurements were made at lab angles of 15° and 30°, and, for each angle, data were obtained alternately to the left and to the right of the incident beam. The electronic system sent the appropriate signals to an on-line computer for mass identification and further processing. The types and amounts of impurities in the gas target were carefully measured by elastic scattering. The impurity concentration amounted to about 10% and was composed principally of hydrogen and helium-3. As has been found previously,[19] the hydrogen concentration slowly increased with time. A test was made to determine whether or not the multiple scattering of the beam α particles in the target windows might lead to incomplete charge collection in the Faraday cup. It was found necessary

to make a small correction for this effect. The $^3H(\alpha,t)^4He$ measurements were made at 18 energies in the resonance region of interest.

C. Reaction: Apparatus and procedure

In Fig. 1 is shown a schematic diagram of the apparatus used for the $^3H(\alpha,^6Li)n$ reaction measurements. The target and triton monitor detectors were situated in a 60-cm cubical scattering chamber[23,24] (not shown in Fig. 1) called the "supercube." The target[25] consisted of a 71-$\mu g/cm^2$ layer of Ti-tritide on a 1.4-mg/cm^2 Ni backing and contained about 1.1 tritium atom per Ti atom. The tritium loading was accomplished by heating the Ni-Ti foil to about 500° C in a tritium atmosphere, causing only the Ti to absorb tritium. The rather thick Ni backing of the target served two purposes. First, the target had to withstand breakage if a vacuum accident were to occur, because contamination of the supercube with small pieces of Ti-tritide could not be tolerated. Second, multiple scattering in the backing disperses the incident α beam to such an extent that only a small fraction of the beam eventually enters the magnet used to detect ^{6}Li ions (see Fig. 1). This greatly reduces the α-particle background in the ^{6}Li detector. During data taking, the target was always oriented so that the recoil tritons and reaction ^{6}Li ions would not have to pass through the Ni backing before being detected.

The monitor detectors consisted of four, ΔE-E detector pairs set at lab angles of ±15° and ±30° to detect elastically recoiling tritons (see Fig. 1). These detectors were collimated with rectangular apertures which subtended a full angular width of 1.2° in the reaction plane. Al foils were inserted between the collimators and the ΔE detectors in order to block the copious flux of α particles elastically scattered mainly by the target backing. Care was taken that no inefficiencies were present in the detection of the tritons due to their multiple scattering either in the Al foils or in the ΔE detectors.

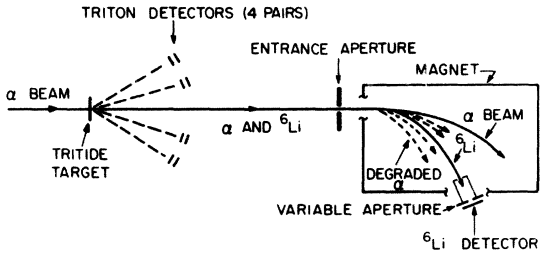

FIG. 1. Schematic diagram of the apparatus for measuring the $^3H(\alpha,^6Li)n$ 0° cross section. The triton detectors monitor the elastic scattering $^3H(\alpha,t)^4He$ at ±15° and ±30°, and the ^{6}Li reaction products are spatially separated from the α-particle beam in the magnet. A thin detector helps to separate in energy the ^{6}Li ions from α-particle background due principally to beam interaction with the entrance aperture.

For this experiment, the Faraday cup and polarimeter of the supercube[23,34] were replaced by a straight section of beam tube to allow the ^{6}Li reaction products to enter a simple dipole magnet[26] (the 0° spectrometer), where they could be spatially separated from the beam α particles. However, because the magnetic rigidity of the α beam was greater than that of the detected ^{6}Li ions, many α particles which lost energy or changed direction through collision processes could still find their way into the ^{6}Li detector (see Fig. 1).

Possible sources of such an α-particle background are as follows: (i) a low-energy component in the incident beam, caused by beam interactions with the beam-line collimators, (ii) beam scattering by the residual gas in the magnet vacuum box, (iii) secondary scattering from the walls of the vacuum box, and (iv) interaction of the α beam with the edge of the magnet entrance aperture (Fig. 1) causing changes in direction and energy degradation of the beam particles. All of these effects were reduced by using a relatively thick target backing, as discussed above. In addition, the effect of (i) was minimized by paying careful attention to beam focusing and collimator sizes, the effect of (ii) was kept reasonably small by keeping the pressure in the vacuum box below about 3×10^{-5} Torr, and the effect of (iii) was minimized by proper baffling of the vacuum box. Item (iv) was found to be the principal source of α-particle background, and therefore studies were made of the background produced by several types of magnet entrance apertures. The materials tested were Al, Ni, Ta, and U, and the thicknesses tested ranged from 50 to 250 μm. All the aperture openings were circular with nominal diameters of 2.6 mm and with highly polished edges. A 50-μm thick Ta aperture was found to give the lowest background and therefore was used in the experiment. An additional antiscattering aperture (not shown in Fig. 1) was also installed at the magnet entrance. The centers of these two apertures were set on the line defining the incident beam direction, which line was determined by sighting with a telescope on the appropriate beam-line collimators.

The ^{6}Li detector assembly was mounted in the side of the 0°-spectrometer vacuum box. It consisted of a six-position wheel, which allowed different aperture types to be placed in position without breaking vacuum, and a collimator snout, which restricted the volume viewed by the ^{6}Li detector and thereby reduced the α-particle background flux into the detector. The placement and alignment of this assembly were checked by ex-

posing photographic paper to an α-particle beam allowed to enter the 0° spectrometer through the entrance aperture.

Two ^{6}Li detectors were used in the experiment. Both were fully depleted Si surface-barrier detectors of sensitive area 50 mm^2. The detector used to detect the high-energy ^{6}Li group was 16.7-μm thick and that used to detect the low-energy ^{6}Li group was 15.3-μm thick. These detectors were thick enough to stop the ^{6}Li groups of interest, but thin enough to allow a reasonably large difference between the ^{6}Li energies and the maximum energies which α particles could deposit in the detectors.

The energy pulses of interest were analyzed in analog-to-digital converters (ADC's), and all the important ancillary pulses were scaled. The outputs of the ADC's and scalers were sent to an on-line computer for recording and processing. Mass identification[27] was performed on the monitor signals only. However, the ^{6}Li-detector signals were sent along with the monitor signals to a mixer-coder,[27] which fed the analog, coding, and gating pulses to the ADC's, so that the combined mixer-coder-ADC dead time was the same for the monitor system and ^{6}Li-detection system. Because of the efforts already mentioned, we were able to reduce the α-particle background to manageable proportions; however, there were still present enough low-pulse-height events from such background to require care in processing the pulses from the ^{6}Li detector. The principal problem caused by these background events was that they could pile up into the spectral region where the ^{6}Li pulses occurred, resulting in a possibly unacceptable uncertainty in the determination of the ^{6}Li yield. This problem was alleviated by using the shortest amplifier[28] clipping time (0.25 μsec) consistent with good resolution for the ^{6}Li peak and by using the lowest beam currents (5–10 nA) consistent with a reasonable rate of data accumulation. Most of the background pulses were prevented from entering the mixer-coder by discriminating against them in a linear gate through which the ^{6}Li-detector pulses were sent on their way to the mixer-coder. In addition, the low-level background was continuously monitored with a fast discriminator and scaler. The output of a pulse generator was fed into the preamplifier for the ^{6}Li detector and was allowed to produce counts in an otherwise unused part of the spectrum. This served as a general check on the operation of the system during data taking; however, its main purpose was to monitor any excessive dead time which might occur in the ^{6}Li-detector electronic circuit from the preamplifier to the mixer-coder. It was felt important to do this because of the relatively large background

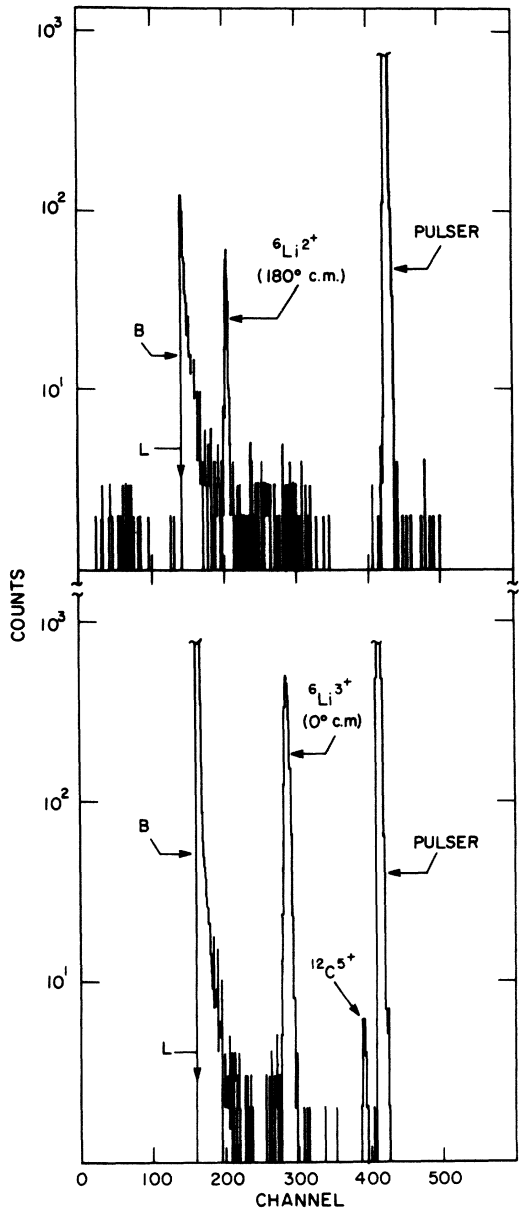

FIG. 2. Sample spectra from the ^{6}Li detector. L indicates the level above which the linear gate allows pulses to pass, B indicates α-particle background, and the pulse-generator peak is also shown. The top figure illustrates detection of a low-energy ^{6}Li group of charge state 2+, and the bottom figure illustrates detection of a high-energy ^{6}Li group of charge state 3+.

rate in that part of the circuit, and, as mentioned in Sec. III B below, it indeed was found necessary to account for this extra dead time for some of the data involving detection of ^{6}Li ions in the 2+ charge state.

Two sample pulse-height spectra from the ^{6}Li detector are shown as semilogarithmic plots in Fig. 2. That portion (B) of the background is

shown which contains pulse heights greater than the level (L) at which the linear gate begins to allow pulses to pass through it. Note that in the upper figure (low-energy ^6Li group, charge state 2+) the background rate was high enough to cause pile up into the region of the ^6Li peak and to produce a small number of "leak-through" pulses below the setting L. In the lower figure (high-energy ^6Li group, charge state 3+) a small but distinct peak from the detection of ^{12}C is present. Occasionally such elastic-recoil ^{12}C or ^{16}O ions from target contamination can occur in the spectrum, and they sometimes can occur moderately close to the ^6Li peak. Care was taken not to include any such events in the extracted ^6Li yield.

The magnet entrance aperture subtended an angle of 0.17° at the target. Since this aperture determines the solid angle for detection of the ^6Li reaction products, it is important to know whether or not all ^6Li ions which entered the 0° spectrometer through it could be detected in the 50-mm^2 detector. The shape and cross-section dimensions of the pencil of ^6Li trajectories entering the detector is determined mainly by two parameters: the diameter of the entrance aperture (about 2.6 mm) and the energy spread of the ^6Li ions caused by the thickness of the Ti-tritide layer of the target (about 80 keV). These parameters were chosen to ensure detection of all ^6Li ions in a given charge state which entered the 0° spectrometer. Even so, several tests were made to investigate the ^6Li detection efficiency, using the aperture wheel in front of the detector. First, the number of ^6Li particles (high-energy group, charge state 3+) detected per 15°, elastic-recoil triton observed in the monitor detectors was measured as a function of magnetic field. This measurement used the largest detector aperture, a 7.6-mm-diam hole, which is slightly smaller than the diameter of the sensitive area of the detector. A flat region, or plateau, was observed in the graph of the ^6Li yield vs spectrometer field. Second, the field was set at the midpoint of the plateau, and two smaller apertures, holes with diameters 6.4 and 5.1 mm, were used to measure the ^6Li yield. These measurements showed that the ^6Li group was well centered on the detector and that the maximum transverse dimension of the ^6Li pencil at the detector was somewhat larger than 5.1 mm but less than 6.4 mm. A third, extremely convenient method was also used for checking yield efficiency. A 6.3-mm-diam disk was supported at four points inside a 7.6-mm-diam hole in the aperture wheel. This produced a nearly annular aperture of width 1.3 mm. When the ^6Li pencil strikes the detector properly, the insertion of the annulus would cause all the ^6Li ions to strike the disk, and the observed yield would vanish. If, on the other hand, the field were set incorrectly or the transverse dimensions of the ^6Li pencil were too large, then some ^6Li yield would be observed from those ions passing through the annular opening. As mentioned below, this annulus was used often during data taking to make sure that the magnetic field setting was correct.

Other diagnostic tests were also performed on the system. By measuring the ^6Li yield at a pressure in the magnet vacuum box an order of magnitude larger than normal, it was shown that charge exchange in the magnet causes no problem. In a further test, the ^6Li yield was measured with and without a C foil inserted immediately behind the target. This showed there was no significant deviation from charge-state equilibrium for the ^6Li ions emerging from the target and, more importantly, that multiple scattering of the ^6Li ions in the target did not significantly affect the yield. Multiple scattering of the incident α particles in the Ni backing before they reach the tritide layer did need to be considered, however. This is discussed below in Sec. III B.

All relevant geometrical quantities were determined accurately. These include all important distances, and the orientations with respect to one another of the monitor detector apertures, the 0°-spectrometer entrance aperture, the optical beam line, the target, and the axes of rotation of the two supercube turntables which hold the monitor detectors. The dimensions of the monitor apertures and magnet entrance aperture were measured with a precision toolmaker's microscope, and the microscope calibration was checked by measuring several standard gauge blocks.

At the beginning of each data-taking period, the α-particle beam was carefully focused and steered to coincide as well as possible with the optically determined 0° line. This process was facilitated both by reading the beam current striking the entrance aperture of the 0° spectrometer and by using a Faraday cup (not shown in Fig. 1) which could be inserted immediately behind this aperture. Current read-out capability for the other collimators in the beam line allowed monitoring of the beam direction during data taking. Especially important in this regard was the current on a set of four-way slits and on the final anti-scattering collimator.

Kinematic relations, target energy loss calculations, and a 0°-spectrometer calibration at one bombarding energy were used to calculate the magnetic field (nuclear-magnetic-resonance frequency) needed to center the appropriate ^6Li group on the detector at each α-particle bombarding energy. In order to check that this calculated field

was indeed correct, the annular aperture was often inserted in front of the detector during the measurements. Each time, the central disk of the annulus was found to block the ^{6}Li group of interest, thereby verifying the correctness of the field setting.

The primary data were obtained by measurement of the yield of the dominant 3+ charge state of ^{6}Li. However, to obtain absolute differential cross sections, the fraction ϕ_2 of ^{6}Li ions produced in the 2+ charge state also had to be determined. This fraction was measured for eight ^{6}Li energies covering the energy range of interest in our experiment. The values we obtained for ϕ_2 are, on the average, 21% higher than the theoretical values given in Ref. 29. We found ϕ_2 to be about 0.08 for the high-energy ^{6}Li group and about 0.14 for the low-energy group. The fractions ϕ_1 and ϕ_0 of ^{6}Li ions produced in the 1+ and neutral charge states, respectively, should be very small,[29] and were assumed negligible.

The yield of the high-energy ^{6}Li group (corresponding to emission at 0° c.m.) was measured at 14 energies from $E_\alpha = 11.310$ to 11.930 MeV (lab), and the yield of the low-energy ^{6}Li group (corresponding to emission at 180° c.m.) was measured at 11 energies in the range from $E_\alpha = 11.415$ to 11.779 MeV (lab). These 25 measurements span the resonance region corresponding to lab neutron energies from $E_n = 0.087$ to 0.398 MeV for the reaction ^{6}Li$(n,t)^4$He.

D. Energy scale

There are two basic problems associated with the energy scale in this experiment. One is the matching of the energy for the reaction experiment (Sec. II C) to that for the separate elastic-scattering experiment (Sec. II B), and the other is the determination of the absolute energy scale. The reaction experiment measures the ratio of the ^{6}Li yield to the elastic-recoil triton yield, and to obtain an absolute differential cross section for the reaction, we used our measurement of the differential cross section for the production of elastic-recoil tritons at 15° (lab). The matching is important because in the energy region of interest, the cross sections show a strong energy dependence. As mentioned in Sec. II A, this energy matching was accomplished by measuring the ratio of the yield of elastic-recoil tritons at 15° (lab) to that at 30° (lab). The energy dependence of this ratio allowed the energies in the two experiments to be matched to within a few keV without knowing independently the energy loss of the incident beam in either target.

Reported values of the energy in the region of the $\frac{5}{2}^-$ resonance at which the ^{6}Li$(n,t)^4$He total reaction cross section has its maximum value vary considerably. For example, the work of Ref. 30 gives a lab neutron energy E_n of about 232 keV for this value, whereas the value quoted in Ref. 4 is 247 keV. We therefore expended considerable effort to determine accurately the reaction energy E_α of the incident α particles in the interaction region of the target. This determination involves the measurement of three quantities: (i) the beam energy, (ii) the beam energy loss in the target, and (iii) the thickness of the Ti-tritide layer on the beam-exit side of the Ni backing.

For item (i), the tandem beam-analyzing magnet was calibrated, yielding a beam energy accurate to 1 or 2 keV. The calibration was carried out by measuring ^{12}C(p,p) elastic scattering in the region of the isospin-forbidden resonance which occurs[31] at a proton lab energy of 14.23075 ± 0.00020 MeV.

For item (ii), the energy losses of 11-, 11.5-, and 12-MeV α particles in the target were measured by using the quadrupole-dipole-dipole-dipole (Q3D) magnetic spectrograph.[32] There we determined the energy difference between α particles scattered from the target of interest and α particles scattered from a very thin (38 μg cm^2) Ni target, and a small correction was made to account for the energy loss in the thin target. The nominal energy loss in the target of interest was about 400 keV, and the actual losses could be measured to about 4 keV. The target uniformity was also studied, and it was determined that nonuniformities cause an additional uncertainty of about 4 keV in the beam energy for the 0° measurements.

For item (iii), the scattering of 14.3-MeV protons at 160° (lab) from the target was used along with the known p+Ti elastic cross section[33] to determine that the Ti layer has a thickness of 71 μg/cm^2. This corresponds to an α-particle energy loss of 20 keV in the 0° experiment. Therefore the reaction energy E_α in the 0° experiment is given by the beam energy, minus the total energy loss in the target, plus 10 keV. Overall, E_α is known to ±6 keV, which corresponds to an uncertainty of ±3 keV in the lab neutron energy E_n for the reaction ^{6}Li$(n,t)^4$He.

III. DATA REDUCTION

A. Elastic

Discussions of procedures for and errors involved in the extraction of differential cross sections from gas-target data are given, for example, in Refs. 17, 18, and 34. Equation (1) of Ref. 34 gives the formula relating the lab differential cross section to measured quantities.

Geometric calculations for gas-target detection systems are carried out in Refs. 21 and 22. In general, the methods of these references, particularly of Ref. 18, were used in reducing the present elastic-scattering data to differential cross sections. Two sets of corrections for the effects of finite geometry, multiple scattering, and beam energy spread need to be considered here. One set serves to correct the gas-target, 15° excitation functions to match the conditions under which the triton elastic recoil data were obtained with the 15° monitor detectors in the supercube during the reaction experiment. The other set serves to correct both of the gas-target excitation functions as completely as possible for these effects in order to present final values for the 15° and 30° elastic differential cross sections.

Finite geometry effects were considered by applying a formula from Ref. 35 to the solid-target data, obtained in the supercube, and by applying a formula from Ref. 21 to the gas-target data. Multiple-scattering effects were considered by using a formula from Ref. 36, and the multiple-scattering of both the α-particle beam and the detected tritons was taken into account. The needed rms multiple-scattering angles (about 1° for the α particles and $\frac{1}{2}$° for the tritons) were calculated by the method of Ref. 37. Although this multiple-scattering formula[36] was derived for solid-target geometry, some studies we have made with Monte Carlo calculations have shown that it is still reasonably accurate when applied to our gas-target geometry. Our use of these formulas required knowledge of σ' and σ'', the first and second derivatives, respectively, of the lab, elastic differential cross section with respect to lab angle. We could not obtain σ' and σ'' from the present experiment because we did not measure angular distributions. Instead, we made use of R-matrix calculations[38] of these quantities based on a fit[16] to a large body of mass-7 data. These considerations showed that the solid-target and gas-target 15° excitation functions could differ by at most 0.1% due to differences in geometry and in multiple-scattering processes, and consequently, no corrections for these effects needed to be made to match the two sets of 15° data. On the other hand, a small correction was made for the difference in beam-energy spread for the two 15° data sets. This correction becomes barely significant only in the region of the excitation-function minimum, which occurs near $E_\alpha = 11.58$ MeV, and amounted to at most 1%. The energy-spread corrections for the elastic data were made with an R-matrix code which produced a good fit to our excitation functions and which contains an energy-folding capability.[38] In these experiments, the energy spread in the beam, when it reaches the reaction region of the target, is almost entirely due to energy straggling in the target. This energy straggling was treated in the Gaussian approximation in which particles of charge z have[39] energy spread (FWHM) $\Delta E = 29.4z \times (xZ/A)^{1/2}$ keV after having passed through a material of atomic number Z, of atomic weight A, and of thickness x in mg/cm^2. The validity here of the Gaussian approximation was verified by performing a modified Vavilov calculation with the computer code STRAGL.[40] The ΔE formula gives $\Delta E = 48$ keV for the reaction experiment using the solid target and $\Delta E = 60$ keV for the elastic-scattering experiment using the gas target. Thus the energy-spread matching consisted in correcting the data obtained with a 60-keV spread to what would have been obtained with a 48-keV spread. This matched, 15°, elastic excitation function was used to normalize the data for the 0° reaction $^3H(\alpha,^6Li)n$, as discussed below in Sec. III B.

To obtain final elastic differential cross sections, the full effects of finite geometry, multiple scattering, and beam-energy spread were unfolded from the gas-target 15° and 30° data. Generally, the corrections for these effects were larger for the 30° data. This is mainly because the 30° excitation function varies more rapidly with energy than does the 15° excitation function and because the angular distributions in our energy range have relative minima near 30°, but not near 15°. The combined corrections for finite geometry and multiple scattering were negligible for the 15° data, but ranged from about 3 to 6% for the 30° data, and the corrections for beam energy straggling ranged from 0 to about 3% for the 15° data and from 0 to about 9% for the 30° data.

We conclude this section with a brief mention of the main sources of error in the elastic cross sections. A thorough discussion of errors arising in the use of the gas-target system is given in Sec. IV of Ref. 18, much of which is relevant to the present measurements. The standard deviation in the absolute cross-section scale is 0.6% and comes from the following contributions: target gas pressure, 0.2%; target gas temperature, 0.1%; target gas purity, 0.4%; detection geometry, 0.2%; and beam current collection, 0.35%. The major contributions to the relative standard deviations in the 30° data are, approximately: counting statistics, 1%, background determination, 1%; multiple-scattering corrections, 1%; and beam-energy-spread corrections, 0.1–1.1%. The major contributions to the relative standard deviations in the 15° data are, approximately: counting statistics, 0.5%; background determination, 0.3%; multiple-scattering corrections, 0.1%; beam-energy-spread corrections, 0.1–0.5%; and absolute angle uncertainty

(0.03°), 0.37%. All compounding of errors was done by adding in quadrature.

B. Reaction

1. Preliminary steps

The first step in reducing the 0° reaction data was to extract the ratio of the number of detected ^{6}Li ions per unit solid angle to the number of detected 15° elastic tritons per unit solid angle. Care was taken to correct for a small amount of mass feed through of deuterons into the triton spectrum and for any α-particle pileup into the region of the ^{6}Li peak. The main error in the yield ratio is from the statistical error in the number of detected ^{6}Li particles, which ranged from 1000 to 5000 in the 3+ charge state and from 200 to 300 in the 2+ charge state. The solid angles were known to ±0.25% and the number of triton counts was known to about ±0.5%.

The second step was to correct the primary data, which was for the 3+ charge state, to account for the ^{6}Li ions produced in the 2+ charge state. This was done by making a linear least-squares fit to the eight measured 2+ probabilities ϕ_2 as a function of ^{6}Li velocity, from which fit a value of ϕ_2 and a correction factor $1/(1-\phi_2)$ were determined for each 3+ measurement. For four of the 2+ measurements, corresponding to detection of the high-energy ^{6}Li group, it was necessary to make an extra dead-time correction in the range 6 to 11%, as determined from the pulser method mentioned in Sec. IIC. The values of ϕ_2 ranged from 0.06 to 0.14 with an error of ±0.005, and this results in an error contribution to the final cross sections of less than 0.6%. Theory indicates[29] that the number of ^{6}Li ions produced in the 1+ and neutral charge states is negligible in this experiment, and thus no corrections for these charge states were made.

The third step was to convert the charge-state-corrected yield ratios to preliminary differential cross sections by using the matched, 15°, elastic differential cross sections referred to in Sec. IIIA. The error in this preliminary reaction cross section was calculated by adding in quadrature the total error in the elastic cross section and the error associated with the uncertainty in the reaction energy E_α (±6 keV). This latter error was computed by multiplying 6 keV by the slope with respect to lab energy of the 15° elastic cross section, and it ranged from negligible to 2%.

2. Multiple-scattering and energy-spread corrections

The preliminary cross sections were corrected for the beam energy spread, due mainly to energy straggling in the target backing, and for the multiple scattering of both the incident α-particle beam in the target backing and the outgoing ^{6}Li ions in the Ti-tritide layer of the target. The latter correction is quite small, but the former two are significant.

The multiple-scattering formula of Ref. 36, which was used to correct the elastic data, is not valid at 0°; however, the correct formula is readily derived. If, as in Ref. 36, we expand the lab cross section through the second derivative term (parabolic approximation), and if we include the effects of beam energy spread, we obtain

$$y = \frac{\langle\sigma\rangle}{\sigma} + \tfrac{1}{2}(\epsilon_\alpha^2 + \epsilon_6^2)\frac{\langle\sigma''\rangle}{\sigma} . \tag{1}$$

In Eq. (1), y is the ratio of the measured ^{6}Li yield to the yield which would have been obtained with no multiple scattering and beam energy spread; ϵ_α and ϵ_6 are the rms multiple-scattering angles[37] for the α particles and ^{6}Li ions, respectively; σ and σ'' are, respectively, the lab cross section and second derivative of the lab cross section with respect to lab angle for the reaction ^{3}H(α,^{6}Li)n at 0°; and the brackets represent smearing over the incident energy. The energy smearing $\langle f\rangle$ for a quantity f which depends on energy E is given by

$$\langle f\rangle \equiv \int_0^\infty f(E)P(E)\,dE , \tag{2}$$

where $P(E)$ is the probability density function for the α-particle beam and is represented by a Gaussian with a FWHM energy spread of 48 keV (see Sec. IIIA). Quantities without brackets in Eq. (1) are to be evaluated at the reaction energy $E_\alpha = \langle E\rangle$. The rms angle ϵ_α was about 0.8° and ϵ_6 was about 0.3°. Because the *full* angular opening of the 0°-spectrometer entrance aperture was only 0.17°, no finite geometry corrections need be included in Eq. (1). To compute the quantity $\langle\sigma''\rangle/\sigma$ in Eq. (1), we used the angular distributions of Ref. 30 for the reaction ^{6}Li(n,t)^{4}He, after conversion to lab cross sections for ^{3}H(α,^{6}Li)n. In doing this, however, it was found necessary to shift the lab neutron energy E_n for the data of Ref. 30 upward by 13 keV in order to bring that energy scale into agreement with ours. The quantity $\langle\sigma\rangle/\sigma$ in Eq. (1) was computed from the results of the present experiment. We examined the validity of the parabolic approximation by comparing multiple-scattering calculations using that approximation with calculations based on full numerical integration. The agreement was good; however, small corrections were applied to Eq. (1) to account for the differences observed.

The final, 0°, lab differential cross sections for ^{3}H(α,^{6}Li)n were obtained by dividing the prelimin-

ary cross sections by the quantity y of Eq. (1). The 25 values of y ranged from about 0.95 to 1.13, and all but 4 of them fell in the range 0.96 to 1.04. The error in y was taken as the larger of 0.005 or 20% of $y-1$. For most of the data, this contributes an error of 0.5–1.0% to the final cross sections.

3. Conversion to $^6Li(n,t)^4He$

For comparison with other work, we have converted our results from lab differential cross sections σ_{lab} for the reaction $^3H(\alpha,^6Li)n$ at $\theta_{lab}=0°$ to c.m. differential cross sections $\sigma_{c.m.}$ for the $^6Li(n,t)^4He$ reaction at $\theta_{c.m.}=0°$ and 180°. We list some of the formulas involved in this conversion, mainly to point out a pitfall to be avoided when dealing with reactions near threshold. Let J_0 be the 0° (lab) Jacobian for converting our lab cross section to the c.m. cross section for $^3H(\alpha,^6Li)n$, or equivalently to the c.m. cross section for $^4He(t,n)^6Li$. This Jacobian is given by

$$J_0=\frac{x_0 R_J}{(1\pm\sqrt{x})^2}, \tag{3}$$

where the plus sign refers to the high-energy ^6Li group, and the minus sign refers to the low-energy ^6Li group, and where

$$x=x_0 R_x, \tag{4}$$

with

$$x_0=\frac{M_t M_n}{M_\alpha M_6}\frac{E_\alpha-E_{th}}{E_\alpha}. \tag{5}$$

In Eqs. (3) and (4), R_J and R_x are relativistic correction factors which are straightforward to derive and which are very close to unity here. In Eq. (5), the quantities M are the appropriate masses, and E_α and E_{th} are, respectively, the lab α-particle and lab threshold energy for the reaction $^3H(\alpha,^6Li)n$. The threshold energy is given by

$$E_{th}=\frac{c^2}{2M_t}[(M_n+M_6)^2-(M_\alpha+M_t)^2]$$
$$=11.1362\ \text{MeV}. \tag{6}$$

When a kinematic expression, such as that of Eq. (3), is written explicitly in terms of E_{th}, it becomes clear that for reactions near threshold it is important that an accurate value of E_{th} be used. Therefore, the correct relativistic relation, as in Eq. (6), should be employed. In such a situation one should avoid using nonrelativistic formulas in which E_{th} is implicit rather than explicit. Such a procedure would be equivalent to using the nonrelativistic expression for E_{th}, and that would lead to unnecessarily large errors in the calculated kinematic quantities. As an example, use of the nonrelativistic value of E_{th} for the present reaction would yield a 4% error in J_0 at an energy E_α of 100 keV above threshold.

Finally, to convert the c.m. cross section for the $^4He(t,n)^6Li$ reaction to the c.m. cross section $\sigma_{c.m.}$ for the $^6Li(n,t)^4He$ reaction, we must multiply by a reciprocity factor $\frac{1}{3}k_t^2/k_n^2$. This yields the overall conversion relation

$$\sigma_{c.m.}=\frac{M_t^2}{3M_6^2}\frac{\sigma_{lab}}{(1\pm\sqrt{x})^2}R_\sigma, \tag{7}$$

where R_σ is a relativistic correction factor which is very close to unity, and x is defined in Eq. (4). Note that the strong dependence on $E_\alpha-E_{th}$ present in Eq. (3) is not present in Eq. (7). This is because the reciprocity factor contains a factor $1/(E_\alpha-E_{th})$ which cancels the term $(E_\alpha-E_{th})$ in J_0. This cancellation is fortunate because the 6-keV error in E_α then causes only an additional uncertainty in $\sigma_{c.m.}$ of about 0.1% over that already contained in σ_{lab}. The lab neutron energy E_n associated with the converted cross section was obtained from the relativistically correct expression

$$E_n=\frac{M_t}{M_6}(E_\alpha-E_{th}). \tag{8}$$

We conclude this section with a brief summary of the error contributions to the final values of $\sigma_{c.m.}$ for the $^6Li(n,t)^4He$ reaction. These standard deviations are, approximately: counting statistics and background determination, 2.3%; charge-state correction, 0.5%; conversion of ratio data to lab differential cross section, 1.5%; multiple-scattering and beam-energy-spread corrections, 0.8%; conversion to c.m. and inverse reaction, 0.1%. All compounding of errors was done by adding in quadrature.

C. Results

The results of the elastic-scattering measurements are given in Table I. The data were obtained as differential cross sections for $^3H(\alpha,t)^4He$ as a function of α-particle lab energy E_α, but are presented as c.m. differential cross sections for $^4He(t,t)^4He$ as a function of triton lab energy E_t.

The results of the reaction measurements are given in Table II. The data were obtained as differential cross sections for $^3H(\alpha,^6Li)n$ as a function of E_α, but are presented as c.m. differential cross sections for $^6Li(n,t)^4He$ as a function of lab neutron energy E_n. A 0.6% scale error, deriving from the scale error in the 15° $\alpha+t$ elastic data, is included in the quoted percent error Δ. If this scale error were to be unfolded from Δ, it would result in a reduction in Δ of at most 0.1%. These reaction results are also shown as solid circles in the graphs of Fig. 3.

TABLE I. Excitation functions for $^3H(\alpha,t)^4He$ at 30° and 15° (lab). The data are presented as c.m. differential cross sections $\sigma_{c.m.}$ for $^4He(t,t)^4He$ at c.m. angles of 119.95° and 149.97° and at triton lab energies E_t. The relative standard deviations Δ are given in percent, and there is an additional 0.6% standard deviation in the absolute cross-section scale. The uncertainty in E_t is ±4.5 keV. The data have been corrected for the effects of finite geometry, multiple scattering, and beam energy spread.

	$\theta_{c.m.}=119.95°$		$\theta_{c.m.}=149.97°$	
E_t (MeV)	$\sigma_{c.m.}$ (mb/sr)	Δ (%)	$\sigma_{c.m.}$ (mb/sr)	Δ (%)
8.507	10.40	1.5	142.14	0.58
8.546	8.89	1.6	139.26	0.58
8.586	7.52	1.6	131.89	0.57
8.625	5.99	1.7	123.30	0.61
8.663	4.53	1.7	111.84	0.63
8.684	3.81	2.1	105.34	0.62
8.704	3.57	1.8	97.25	0.76
8.724	3.95	1.9	95.77	0.71
8.743	5.72	2.0	98.30	0.66
8.763	8.19	1.8	106.05	0.78
8.782	10.19	1.5	115.32	0.76
8.801	11.18	1.4	125.02	0.67
8.822	11.55	1.5	133.10	0.65
8.841	11.74	1.5	137.70	0.59
8.861	11.60	1.5	142.58	0.57
8.898	10.78	1.5	144.50	0.59
8.975	9.31	1.6	140.97	0.60
9.050	8.10	1.7	137.13	0.59

TABLE II. Excitation functions for $^3H(\alpha,^6Li)n$ at 0° (lab). The data are presented as c.m. differential cross sections $\sigma_{c.m.}$, along with their total standard deviations Δ, for the reaction $^6Li(n,t)^4He$ at c.m. angles of 0° and 180° and at lab neutron energies E_n. The uncertainty in E_n is ±3 keV. The data have been corrected for multiple scattering and beam energy spread.

	$\theta_{c.m.}=0°$		$\theta_{c.m.}=180°$	
E_n (keV)	$\sigma_{c.m.}$ (mb/sr)	Δ (%)	$\sigma_{c.m.}$ (mb/sr)	Δ (%)
87	90.9	3.0	...	...
113	103.9	3.2	...	...
140	122.9	2.6	31.0	5.7
165	179.4	2.6	71.8	3.7
191	259.8	2.3	150.0	3.0
204	341.8	2.7	210.6	2.9
218	409.9	1.8	268.2	2.3
232	496.1	2.0	348.6	2.4
244	499.8	2.8	380.6	3.1
257	438.1	2.8	375.6	2.9
270	371.2	2.8	345.8	2.9
296	233.5	2.4	232.3	2.8
322	175.7	2.4	148.3	2.9
398	84.1	2.7	...	...

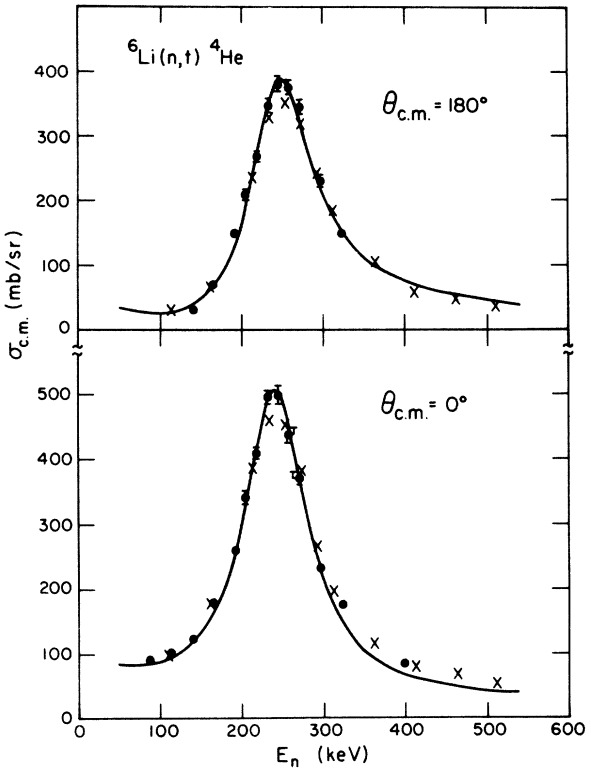

FIG. 3. Differential cross sections $\sigma_{c.m.}$ vs lab neutron energy E_n for $^6Li(n,t)^4He$. The solid points show the present data, the crosses depict results from Ref. 30 (shifted in energy), and the curves show calculations from the R-matrix fit of Ref. 16.

IV. COMPARISONS WITH OTHER DATA AND EVALUATIONS

The bulk of the published data on the $^6Li(n,t)^4He$ reaction is for the integrated cross section σ vs lab neutron energy E_n. In order to make an approximate comparison of our results with such data, we have used the work of Refs. 30 and 16 to aid in making appropriate conversions of our data. In Ref. 30, Overley, Sealock, and Ehlers have given results of measurements of differential cross sections for $^6Li(n,t)^4He$ for values of E_n from 100 to 1800 keV. They present the data by listing, as a function of E_n, the coefficients B_l (for $l=0$–4) of Legendre-polynomial expansions of the differential cross sections. From these coefficients we calculated the integrated cross section σ ($4\pi B_0$), the 0° differential cross section ($\sum B_l$), and the 180° differential cross section [$\sum(-1)^l B_l$] vs E_n. From these we obtained the ratio of the maximum integrated cross section to both the maximum 0° cross section and the maximum 180° cross section (these maxima do not all occur at the same E_n). We then multiplied these ratios by our 0° and 180° differential cross sections. These

two results for "our" peak value of σ were both very close to 3.15 b, and this value is listed in Table III along with results from other work. We have also listed in Table III the values of E_n at which σ was found to have its peak value. Our value was found with the aid of the R-matrix analysis of Hale and Dodder.[16] That analysis indicates[38] that the integrated cross section should peak about 1.5 keV higher than does the 0° cross section. Since our 0° cross section peaks near 239.5 keV, we obtain 241 keV as our best estimate for the value of E_n at which σ passes through its maximum. On taking approximate account of the errors involved in the σ and E_n values of Table III, we conclude that we are in reasonable agreement with the results of Refs. 5, 16, 42, and 43 and in disagreement with the others.

Our data can be compared directly with some other differential-cross-section results. The work of Ref. 30 has already been mentioned, and the 0° and 180° differential cross sections from that work, as computed from the given Legendre coefficients, are plotted as crosses in Fig. 3. As mentioned above, the energies E_n of Ref. 30 had to be increased by 13 keV to agree with our energy scale.[45] After this energy shift is made, the data of Ref. 30 are in rather good agreement with ours, except for the cross sections near the peaks.

In Ref. 42, Fort has given Legendre coefficients vs neutron energy E_n derived from a two-channel, R-matrix evaluation of $^6Li(n,t)^4He$ data. The 0° and 180° differential cross sections calculated from these coefficients are not shown in Fig. 3, but have the following features. The 0° results of Ref. 42 must be lowered by about 6 keV to bring the peak energy into agreement with ours. When this is done, the 0° cross section of Ref. 42 agrees with ours in the region of the peak, but falls below our data at both the higher and lower energies. The 180° results of Ref. 42 must be raised by about 6 keV to bring the peak energy into agreement with ours. When this is done, the 180° cross section of Ref. 42 falls below ours for energies above 190 keV and falls above ours for energies below this. Overall, the evaluation of Ref. 42 is not in very good agreement with our data.

Our final comparison is with a recent,[16] three-channel,[46] multilevel, R-matrix fit to a large body of mass-7 data. (The present data were not included in the input to the fit.) The 0° and 180° cross sections resulting from this fit are shown as solid curves in Fig. 3. The most obvious discrepancy between the fit and our data is that the 0° R-matrix cross section is lower than the data for E_n greater than about 300 keV. In addition, there is some indication that the 180° R-matrix cross section peaks at a slightly lower energy than the data. However, the overall agreement of this calculation with our data is good.

TABLE III. Comparisons of values of the integrated cross section σ for the $^6Li(n,t)^4He$ reaction at the peak of the $\frac{5}{2}^-$ resonance and of values of the lab neutron energy E_n at which this maximum in σ occurs. Only a portion of the existing data is presented, and Ref. 4 should be consulted for references to other results. The σ values have been extracted from the indicated references to the nearest 0.05 b, and the E_n values have been extracted to the nearest 1 keV. The original references should be consulted for an assessment of the errors in these quantities.

Peak σ (b)	Peak E_n (keV)	Ref.
2.30	255	41
3.45	247	4[a]
3.15	242	42[b]
2.95	241	43
3.00	244	5
2.90	232	30
3.80	252	44
3.25	241	16[c]
3.15	241	Present work[d]

[a] Review and evaluation.
[b] Two channel, R-matrix evaluation.
[c] Three channel, R-matrix evaluation.
[d] Deduced with the help of Refs. 30 and 16. See Sec. IV.

V. CONCLUSION

In Tables I and II we have presented the results of our measured differential elastic-scattering and reaction excitation functions for the mass-7 system in the region of the $\frac{5}{2}^-$ state near 7.46 MeV in ^7Li. Particular attention was paid to problems peculiar to this experiment, especially to the reaction experiment. These include cleanly separating the ^6Li ions from the α-particle beam, accounting for the mixed charge state of the ^6Li ions, and determining the beam energy to obtain the absolute normalization of the cross section. Where necessary, we have corrected our data for finite detection geometry, multiple scattering, and beam energy spread.

We have seen that our data suggest that the integrated cross section σ for $^6Li(n,t)^4He$ should peak near a neutron lab energy of 241 keV and that the peak σ should be about 3.15 b (Table III). Comparisons with other data and evaluations have shown that our 0° and 180° differential cross sections for $^6Li(n,t)^4He$ are in best agreement with a recent,[16] three-channel, multilevel, R-matrix analysis of much of the existing mass-7 data. It should prove valuable to include both the elastic and reaction data of the present experiment in future such analyses.[38]

ACKNOWLEDGMENTS

We express our gratitude to B. Roybal and R. Gill for help with design and construction of apparatus for the experiment, to L. J. Morrison for expert technical assistance with many aspects of the work, to D. H. W. Carstens and J. C. Gursky for making the targets, to J. M. Sunier and R. V Poore for help with the computer system, to E. R. Flynn and S. D. Orbesen for aid in using the Q3D spectrometer, and to the accelerator operators for their diligence in running the FN tandem. For stimulating discussions we thank G. M. Hale, D. C. Dodder, H. T. Motz, R. B. Perkins, L. Stewart, and P. G. Young. In addition, we are grateful to G. M. Hale for performing the R-matrix calculations for us.

---

*Work supported by the U. S. Energy Research and Development Administration.

†Visiting Staff Member from the University of Minnesota, Minneapolis, Minnesota 55455.

[1]*Neutron Standards and Flux Normalization*, proceedings of a symposium at Argonne National Laboratory, 1970, edited by A. B. Smith (U.S. Atomic Energy Commission, Division of Technical Information, Washington, D. C., 1971), Session II.

[2]*Neutron Standard Reference Data*, proceedings of a panel meeting at Vienna, 1972 (International Atomic Energy Agency, Vienna, 1974), Sec. III A.

[3]*Nuclear Cross Sections and Technology*, proceedings of a conference at Washington, D. C., 1975, edited by R. A. Schrack and C. D. Bowman (NBS-425, U. S. Government Printing Office, Washington, D. C., 1975).

[4]C. A. Uttley, M. G. Sowerby, B. H. Patrick, and E. R. Rae, Ref. 1, p. 80.

[5]W. P. Poenitz, Z. Phys. 268, 359 (1974).

[6]R. L. Macklin, N. W. Hill, and B. J. Allen, Nucl. Instrum. Methods 96, 509 (1971).

[7]R. L. Macklin, J. Halperin, and R. R. Winters, Phys. Rev. C 11, 1270 (1975).

[8]T. A. Tombrello, Ref. 3, Vol. II, p. 659.

[9]C. M. Bartle, Ref. 3, Vol. II, p. 688.

[10]J. A. Koepke, R. E. Brown, Y. C. Tang, and D. R. Thompson, Phys. Rev. C 9, 823 (1974), and references therein.

[11]A. M. Lane and R. G. Thomas, Rev. Mod. Phys. 30, 257 (1958).

[12]G. M. Hale, Ref. 3, Vol. I, p. 302.

[13]D. C. Dodder, G. M. Hale, R. A. Nisley, K. Witte, and P. G. Young, Los Alamos Scientific Laboratory Report No. LA-UR-74-738, 1974 (unpublished).

[14]D. C. Dodder, in *Proceedings of the Fourth International Symposium on Polarization Phenomena in Nuclear Reactions, Zurich, 1975*, edited by W. Grüebler and V. König (Birkhäuser, Basel, Switzerland, 1976), p. 167.

[15]R. J. Spiger and T. A. Tombrello, Phys. Rev. 163, 964 (1967).

[16]G. M. Hale and D. C. Dodder, in *Proceedings of the International Conference on the Interactions of Neutrons with Nuclei, Lowell, Massachusetts, 1976,* edited by E. Sheldon [ERDA Report No. CONF-760715 (available from the National Technical Information Service, U. S. Dept. of Commerce, Springfield, Virginia 22161], Vol. 2, p. 1459.

[17]J. L. Detch, Jr., Ph.D. thesis, University of Wyoming, 1970 (unpublished); Los Alamos Scientific Laboratory Report No. LA-4576 (unpublished).

[18]N. Jarmie, J. H. Jett, J. L. Detch, Jr., and R. L. Hutson, Phys. Rev. C 3, 10 (1971).

[19]J. L. Detch, Jr., R. L. Hutson, N. Jarmie, and J. H. Jett, Phys. Rev. C 4, 52 (1971).

[20]Co-rich alloy; Hamilton Watch Co., Lancaster, Pennsylvania 17604.

[21]E. A. Silverstein, Nucl. Instrum. Methods 4, 53 (1959).

[22]J. T. C. Kan, Rev. Sci. Instrum. 44, 323 (1973).

[23]P. A. Lovoi, Ph.D. thesis, University of New Mexico, 1975 (unpublished); Los Alamos Scientific Laboratory Report No. LA-6041-T (unpublished).

[24]G. G. Ohlsen and P. A. Lovoi, in *Proceedings of the Fourth International Symposium on Polarization Phenomena in Nuclear Reactions, Zurich, 1975* (see Ref. 14), p. 907.

[25]The target was fabricated by J. C. Gursky and D. H. W. Carstens.

[26]This is the same magnet used in some previous polarization-transfer studies [G. D. Salzman, G. G. Ohlsen, J. C. Martin, and J. J. Jarmer, Nucl. Phys. A222, 512 (1974)].

[27]D. D. Armstrong, J. G. Beery, E. R. Flynn, W. S. Hall, P. W. Keaton, Jr., and M. P. Kellogg, Nucl. Instrum. Methods 70, 69 (1969).

[28]Model 452 Spectroscopy Amplifier, Ortec, Oak Ridge, Tennessee 37830.

[29]J. B. Marion and F. C. Young, *Nuclear Reaction Analysis Graphs and Tables* (North-Holland, Amsterdam, 1968), p. 38.

[30]J. C. Overley, R. M. Sealock, and D. H. Ehlers, Nucl. Phys. A221, 573 (1974).

[31]E. Huenges, H. Rösler, and H. Vonach, Phys. Lett. 46B, 361 (1973).

[32]E. R. Flynn, S. Orbesen, J. D. Sherman, J. W. Sunier, and R. Woods, Nucl. Instrum. Methods 128, 35 (1975).

[33]C. Hu, K. Kikuchi, S. Kobayashi, K. Matsuda, Y. Nagahara, Y. Oda, N. Takano, M. Takeda, and T. Yamazaki, J. Phys. Soc. Jpn. 14, 861 (1959); D. B. Smith, N. Jarmie, and J. D. Seagrave, Los Alamos Scientific Laboratory Report No. LA-2424 (unpublished) (available from the Office of Technical Services, U. S. Department of Commerce, Washington, D. C. 1960), p. 109.

[34]W. S. Chien and R. E. Brown, Phys. Rev. C 10, 1767 (1974).

[35]I. E. Dayton and G. Schrank, Phys. Rev. 101, 1358 (1956).

[36]C. T. Chase and R. T. Cox, Phys. Rev. 58, 243 (1940).

[37]J. B. Marion and B. A. Zimmerman, Nucl. Instrum. Methods 51, 93 (1967).

[38]G. M. Hale (private communication).
[39]N. Bohr, Phil. Mag. 30, 581 (1915); H. A. Bethe and J. Ashkin, in *Experimental Nuclear Physics*, edited by E. Segrè (Wiley, New York, 1953), Vol. I, p. 166.
[40]R. G. Clarkson and N. Jarmie, Comp. Phys. Comm. 2, 433 (1971).
[41]S. Schwarz, L. G. Strömberg, and A. Bergström, Nucl. Phys. 63, 593 (1965).
[42]E. Fort, Ref. 2, p. 119.
[43]M. S. Coates, G. J. Hunt, and C. A. Uttley, Ref. 2, p. 105.
[44]S. J. Friesenhahn, V. J. Orphan, A. D. Carlson, M. P. Fricke, and W. M. Lopez, Intelcom Rad Tech Report No. INTEL-RT-7011-001 (unpublished); and Ref. 3, Vol. I., p. 232.
[45]The fact that Table III indicates an energy shift of 9 keV for σ rather than 13 keV means that in Ref. 30 the dependence of the peak energy on angle is different from that in Ref. 16.
[46]The included channels are as follows: $\alpha+t$, $n+^6$Li (g.s.), and $n+^6$Li(2.19 MeV).